NeuroImage 236 (2021) 118081

Contents lists available at ScienceDirect

NeuroImage

journal homepage: www.elsevier.com/locate/neuroimage

The parahippocampal place area and hippocampus encode the spatial significance of landmark objects

Liwei Sun [a,b,c,f,1,*], Sebastian M. Frank [b,d,1], Russell A. Epstein [e], Peter U. Tse [b]

[a] Beijing Advanced Innovation Center for Big Data-Based Precision Medicine, Capital Medical University, Beijing 100069, China
[b] Department of Psychological and Brain Sciences, Dartmouth College, Hanover, NH 03755, USA
[c] School of Biomedical Engineering, Capital Medical University, Beijing 100069, China
[d] Department of Cognitive, Linguistic, and Psychological Sciences, Brown University, Providence, RI 02912, USA
[e] Department of Psychology, University of Pennsylvania, Philadelphia, PA 19104, USA
[f] Beijing Key Laboratory of Fundamental Research on Biomechanics in Clinical Application, Capital Medical University, Beijing 100069, China

ARTICLE INFO

Keywords:
Hippocampus
Parahippocampal place area
Landmark
Navigation
Spatial learning

ABSTRACT

Landmark objects are points of reference that can anchor one's internal cognitive map to the external world while navigating. They are especially useful in indoor environments where other cues such as spatial geometries are often similar across locations. We used functional magnetic resonance imaging (fMRI) and multivariate pattern analysis (MVPA) to understand how the spatial significance of landmark objects is represented in the human brain. Participants learned the spatial layout of a virtual building with arbitrary objects as unique landmarks in each room during a navigation task. They were scanned while viewing the objects before and after learning. MVPA revealed that the neural representation of landmark objects in the right parahippocampal place area (rPPA) and the hippocampus transformed systematically according to their locations. Specifically, objects in different rooms became more distinguishable than objects in the same room. These results demonstrate that rPPA and the hippocampus encode the spatial significance of landmark objects in indoor spaces.

1. Introduction

When navigating, perceptible features of the environment allow us to determine where we are and which direction we are facing (Chan et al., 2012). Behavioral work in humans and animals suggests that both geometric cues (e.g. the spatial arrangement of topographical features) and non-geometric cues (e.g. landmark objects) support spatial orientation (Julian et al., 2018). In outdoor settings, the geometry of the landscape provides a strong cue to the location of the observer in space. For many indoor spaces, however, the geometry of subspaces (rooms) can be very similar. In such environments, landmark objects become especially important for discriminating between otherwise indistinguishable subspaces.

How are landmark objects represented in the brain? Previous work suggests that when an object obtains the status of a landmark, it recruits not only object-responsive regions such as the lateral occipital complex (LOC; Malach et al., 1995), but also scene-responsive regions (for a review, see Epstein and Baker, 2019), such as the parahippocampal place area (PPA; Epstein and Kanwisher, 1998), retrosplenial complex (RSC; O'Craven and Kanwisher, 2000), and the occipital place area (OPA; Nakamura et al., 2000). Specifically, scene regions show enhanced responses to objects with qualities that would make them more suitable as landmarks (Troiani et al., 2014), such as being large in size (Konkle and Oliva, 2012), fixed in space (Auger et al., 2015; Auger and Maguire, 2013), or associated with navigationally relevant locations (Janzen and van Turennout, 2004; Schinazi and Epstein, 2010).

Although these results are intriguing, they do not provide direct evidence that scene regions represent landmark objects qua landmarks. For this, it is necessary to show that these brain regions represent a key feature of a landmark: association with a given location (or direction). One study investigated this question by examining multivoxel fMRI responses while participants viewed interior and exterior views of familiar campus buildings (Marchette et al., 2015). Views corresponding to the same building elicited similar multivoxel codes in PPA, RSC, and OPA. This finding was interpreted as evidence for landmark coding, but it was unclear whether the codes related to object identity (i.e. same building) or place identity (i.e. same location). To unconfound these possibilities, one must test whether a shared encoding exists for two different landmark objects located in the same place. Other studies reported evidence for coding of object locations in RSC (Marchette et al., 2014; Persichetti and Dilks, 2019) and hippocampus (Deuker et al., 2016; Morgan et al., 2011; Nielson et al., 2015), by showing similarity or adap-

* Corresponding author.
E-mail address: sunliwei@ccmu.edu.cn (L. Sun).
[1] Liwei Sun and Sebastian Frank contributed equally to this project.

https://doi.org/10.1016/j.neuroimage.2021.118081.
Received 3 January 2021; Received in revised form 13 March 2021; Accepted 12 April 2021
Available online 18 April 2021.

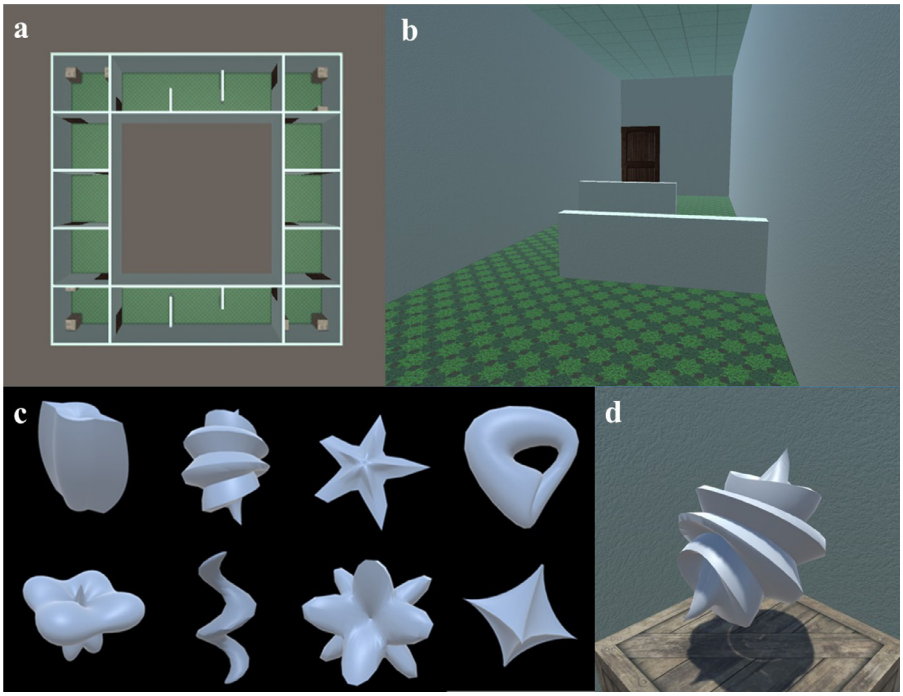

Fig. 1. Stimuli and virtual environment design. a) Aerial view of the virtual-reality space. b) First-person view of the corridor room with obstacles. Participants were forced to walk around the obstacles to reach the door on the other end. They could pass through the doors without delay. c) Artificial objects used in the experiment. Each object had unique geometrical features. d) An example object presented during scanning. During presentation the object was rotating at a constant speed, similar to the training sessions outside the scanner.

tation effects that relate to the distances between the objects. However, these studies suffer from the complementary problem to the one above: it is unclear whether the location codes observed in these regions are general spatial codes, or specific to landmark objects.

To disentangle these issues, here we examined how the human brain learns to encode objects as spatial landmarks in an indoor environment. Participants learned the layout of a virtual building that was symmetric and appeared to be the same from each corner of the building (Fig. 1a). Eight distinct artificial objects were placed in the four corner rooms of the building as the only landmarks. In order to effectively navigate through the building, participants had to learn the location of each object. They were scanned with fMRI before and after learning while they viewed the eight objects in the absence of any spatial task. The neural representations of the objects were compared between the pre and post fMRI sessions. Multivariate classification analyses (Haxby et al., 2001) of the fMRI data were carried out based on object identity (i.e. which object is which) and object location (i.e. which room the objects were in). If the classification accuracy for object location increases and goes above chance level after learning, then it can be inferred that the objects acquired new neural representations in the brain based on their locations in the virtual building.

2. Methods

2.1. Participants

A total of n = 21 participants (12 females; 20–35 years old) from the Dartmouth College community gave informed written consent to participate in the study for monetary reward. The sample size of this study was determined based on a previous study (Marchette et al., 2015). We first calculated the effect size of the previous study (Cohen's $d = 0.778$), and then estimated the required sample size using G*Power (Version 3.1.9.7; Faul et al., 2007) with default parameters ($\alpha = 0.05$, 1- $\beta = 0.95$), which resulted in a sample size of $n = 20$. We also conducted a sensitivity analysis to calculate the minimal effect size that could be detected under different sample sizes around $n = 20$ (Table S1). The minimal effect size for $n = 18$ is 0.81, which is close to what was observed in Marchette et al. (2015; Cohen's $d = 0.778$).

One participant was excluded from the analysis due to excessive head movements during fMRI data collection. Two participants were excluded because none of their functional ROIs could be defined from localizer runs. Therefore, a total number of n = 18 participants were included in the analysis. Participants had normal or corrected-to-normal vision. The study was approved by the Committee for the Protection of Human Subjects at Dartmouth College.

2.2. Stimuli

A virtual-reality space was built with the Unity game engine (Unity Technologies, California; Fig. 1a). The space consisted of the interior of a building with four 4 m × 4 m corner rooms. The four corner rooms were connected by four 12 m × 4 m corridors of the same length and size. Two of the corridors were divided into three 4 m × 4 m small rooms by walls, while the other two corridors were open spaces containing two low obstacles (1 m high, Fig. 1b). All doors between rooms could be passed through directly without any impediment. The arrangement of doors and obstacles forced participants to zigzag in the same way through each corridor. Note that in this design, neighboring corner rooms had the same Euclidean and path distance from each other.

Each corner room included two 0.8 m × 0.8 m × 0.8 m boxes. Each box contained a unique novel object. Another two boxes were put below the boxes with objects as platforms. There were eight objects in total (Fig. 1c). The objects were built from unique mathematical equations and visualized to three-dimensional models by K3DSurf (Version 0.6.2; Taha, 2014). The objects were randomly assigned to boxes for each participant. These location assignments remained constant across the whole experiment.

An important aspect of this environment was that it had a symmetric layout: each corner room and each pair of corridors were geometrically identical. Furthermore, wallpaper patterns, ceilings, floors, textures of the doors, and textures of the boxes were identical across all rooms. Given the geometric symmetry of the scene, the only way participants could uniquely identify their location was by using the objects as landmarks.

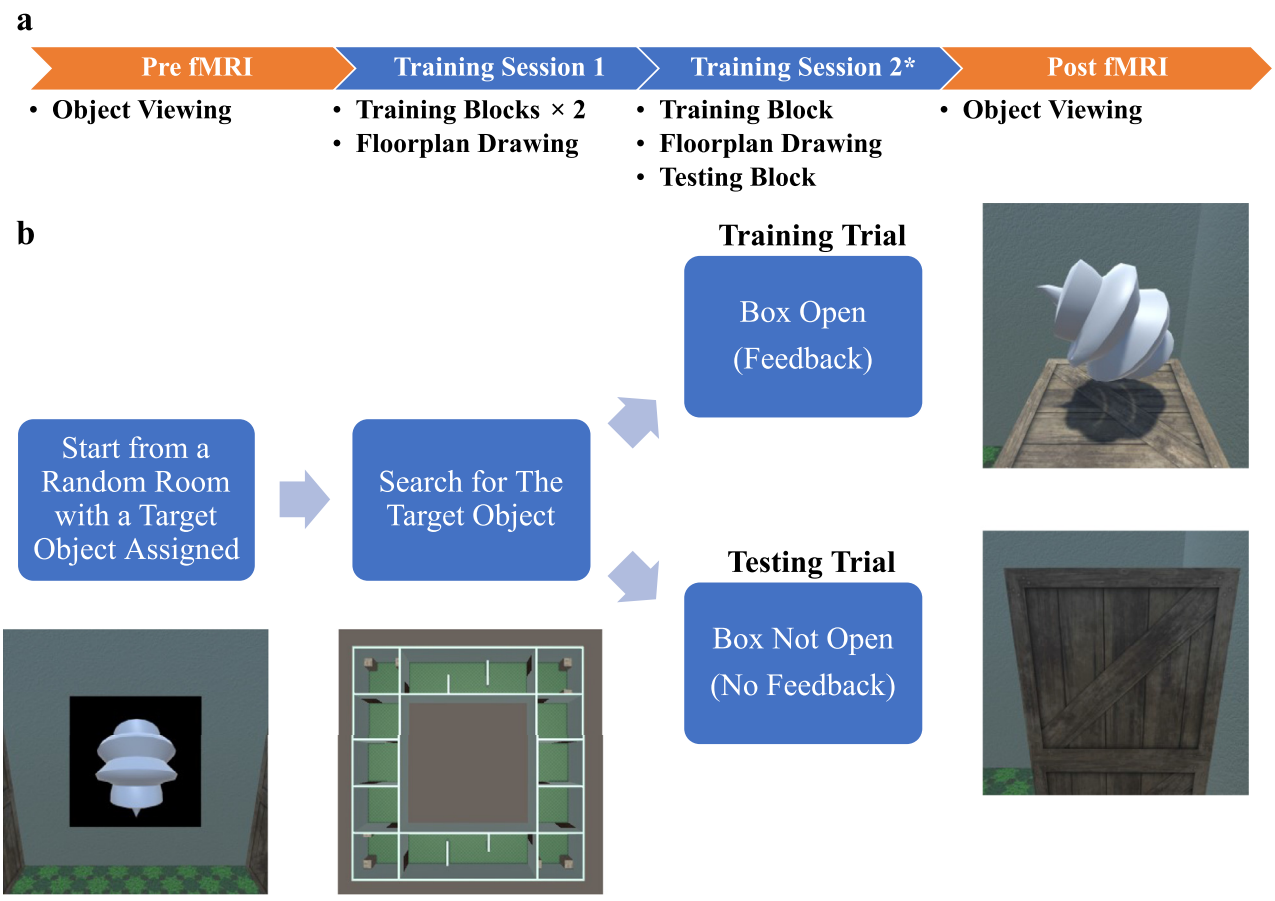

Fig. 2. Experiment design. a) There was a minimum of two training sessions on separate days in the experiment. *More training sessions were included if participants did not reach the expected task performance. Each training or testing block contained 24 trials with tasks described in b). Participants were also asked to draw a detailed floorplan with object locations marked. Before the first and after the last training sessions, participants were scanned with fMRI while viewing the objects in the absence of any spatial tasks. b) Participants were trained on an object search task in order to learn the layout of the virtual building. During training trials, participants were able to open every box in order to identify the object in it. During testing trials, participants could only open the boxes in the room they began with to identify their starting location. After hitting a presumed target box, the box would not be opened and the next trial started immediately thereafter.

2.3. Procedure

The experiment included two fMRI sessions and multiple behavioral training sessions, which were conducted on separate days. In the first and last sessions (referred to as 'pre' and 'post' in the following), fMRI measurements were conducted while participants viewed the objects without spatial context. Between pre and post scans, participants were trained outside the scanner on the layout of the virtual space and the association of different rooms with different objects. The training sessions included a series of training trials and testing trials. The procedure is schematized in Fig. 2.

During each training trial, participants started in a random corner room and were shown the image of a random target object, which was in one of the other three corner rooms. Their task was to walk to the target object via the shortest route. Participants walked from a first-person perspective and could move freely in the virtual building, with no time limit. All objects were covered by boxes. To see the object inside a box, participants had to stand in front of the box and press the space bar. The object was then shown slowly rotating (72 degrees per second), thus providing a full view of the shape of the 3D object. Once participants opened the box with the target object, the program paused for three seconds and then teleported participants to a new starting corner room for the next trial. Participants could press the escape key at any time to review the image of the current target object. They were encouraged to remember the locations of all objects and to open as few boxes as possible to reach the target object. They were also advised to open one of the boxes in the starting room to identify their location, and then to recall the location of the target object relative to the beginning room. Each block of the training session contained twenty-four trials, representing a full combination of four starting rooms and six objects outside the starting room.

Two testing tasks were designed to evaluate participants' progress during training. The first testing task was very similar to the training trial described above. On each trial participants were teleported to one of the corner rooms and given a target object to look for. They could open both boxes in their starting room in order to identify their starting location. However, they were given only one chance to choose one of the other six boxes (i.e. in one of the other corner rooms) to indicate the location of the target object. They were not given feedback on their choice. After participants had pressed the space bar indicating the box with the target object, the box did not open, and they were teleported to another starting room for the next trial. This testing task served as a pure evaluation of the spatial knowledge participants currently had. Each block of the testing task contained twenty-four trials.

The second testing task was to draw a floorplan of the virtual building on paper with a pen. Note that participants never saw the virtual environment from a bird's-eye view during training. Participants were asked to draw a detailed map of the space. Specifically, they had to indicate the exact locations of doors, obstacles, and boxes. To fulfill this task, they were presented with the pictures of all eight ob-

jects. Each picture was marked with a random integer or letter. Participants were then requested to mark the location of each object in the building using corresponding integers or letters. No feedback was given.

The training stage ranged from two to five days. Each training session was conducted on a separate day and took about an hour to complete. Although the timeline of training was not strictly controlled, the last training session had to be scheduled right before the day of the post fMRI session. All participants finished their training within two weeks. On the first day, participants were requested to complete two training blocks followed by a floorplan drawing test. Starting from the second day, participants would do one training block and one testing block with a floorplan drawing test between the two blocks. The training stage ended when participants achieved an accuracy of 100% in both the testing block and the floorplan drawing test. For the map drawing test, accuracy was evaluated based on the correct arrangement of walls and doors. Furthermore, the location of objects in each corner room had to be specified correctly. The exact scale of the environment was not required.

2.4. MRI acquisition

Functional MRI data were acquired on a Siemens 3T Prisma scanner with a 32-channel head coil, located at the Dartmouth College brain imaging center. The T1-weighted structural image was collected using an MPRAGE protocol (repetition time (TR) = 2.35 ms, echo time (TE) = 2.32 ms, flip angle = 8°, matrix size = 192 × 256 × 256, voxel size = 0.9 mm × 0.9 mm × 0.9 mm). The functional MR images were collected with a gradient echo planar imaging sequence (TR = 2000 ms, TE = 35 ms, flip angle = 75°, matrix size = 68 × 68 × 33, voxel size = 3.5 mm × 3.5 mm × 3.5 mm).

This study included two separate fMRI sessions, one before and one after the behavioral training. The procedures and sequences of the pre and post fMRI sessions were identical. In each fMRI session participants saw movies of eight objects rotating (72 degrees per second) in the virtual-reality space (Fig. 1d).

During each fMRI run there were three different types of trials: same-object trials, different-object trials (catch trials), and null trials. Each trial was six seconds long. In same-object trials, three different movies of the same object rotating were presented in a successive sequence with 1 s for each movie, followed by a 3 s inter-trial interval with a blank screen. Different-object trials were the same as same-object trials except the third movie was replaced by a movie of another object. The objects presented in different-object trials were randomly selected. In both same- and different-object trials, participants were requested to press a button during the inter-trial interval to indicate whether the objects shown were the same or different. Different-object trials served as catch trials in order to keep participants focused. Null trials included a blank screen of 6 s. Two null trials were always presented successively (double blanks, 12 s in total). Eight same-object trials (one for each object), one different-object trial, and two consecutive null trials (double blanks) were counterbalanced using a Type-1-Index-1 sequence (Aguirre et al., 2011). This design is similar to the approach used by Connolly et al. (2016).

The Type-1-Index-1 sequence was broken into six separate runs. Each run contained 55 trials, which included 5 same-object trials for each object (40 in total), 5 different-object trials, and 10 null trials (5 double blanks). The beginning of each run included a 12 s blank period and the last 3 trials from the previous run, which helped to link the carryover BOLD signals between the runs. The blank and carryover trials were discarded later in the analysis. At the end of each run the last trial was repeated one more time and another 12 s of blanks were included for the delay of the BOLD signal. Each run lasted for 6 min 18 s.

Participants practiced one run of the experiment on a computer outside the scanner in both pre- and post-scans. The structural T1 scan was collected during the pre-scan, while two functional localizer runs were conducted in the post-scan. Functional localizer runs were conducted to define regions of interest (ROIs) in the LOC, PPA, RSC, and OPA, following previous descriptions (Marchette et al., 2015). During the localizer runs, participants viewed random sequences of pictures of objects, scrambled objects, and outdoor scenes. Those three categories were presented in separate 15-s blocks at a rate of one second per image. Participants were asked to press a button to report 1-back repeated images. This task ensured that participants remained focused during the localizer experiment. Each block was followed by a 15-s blank period between blocks. There were nine blocks of stimulation in total (three for each visual category). Each run lasted for 4 min 30 s.

2.5. Data preprocessing and feature extraction

MRI data were processed using FSL 6.0 (FMRIB, Oxford, UK; Jenkinson et al., 2012). Preprocessing of the functional MRI data of the main experiment included brain extraction, slice timing correction, motion correction, and high-pass filtering to account for the MRI scanner drift. No spatial smoothing was performed. Each run was aligned to the participant's T1-weighted structural image using FSL FLIRT (Jenkinson et al., 2002; Jenkinson and Smith, 2001). The first 15 volumes of each run were discarded. A general linear model (GLM) was conducted to retrieve each voxel's response to the eight objects using FSL FEAT (Woolrich et al., 2001). Beside the eight regressors for the eight objects, a nuisance regressor for the different-object trial was included in the GLM model. Each regressor was convolved with a double-gamma hemodynamic response function (HRF). The temporal derivative of each regressor was also included in the model.

Separate GLMs were conducted for each fMRI run and each participant. In this way, eight parameter estimation (PE) maps, each corresponding to the fMRI response to one object, were generated for each run and each participant. They were voxel-wise normalized to z-scores within each run, and then served as the inputs for the following multivariate pattern analysis.

2.6. ROI definition

ROIs were defined based on activations in the functional localizer runs. Functional MRI data from the localizers were preprocessed as described above for the main experiment, except that images were also spatially smoothed with a Gaussian kernel of 5 mm (full width at half maximum, FWHM). A GLM analysis was carried out to identify voxels that responded to scenes and objects. Three boxcar regressors for scenes, objects, and scrambled objects were convolved with a double-gamma HRF. Two contrasts, scenes versus objects and objects versus scrambled objects, were calculated. The contrasts from the two localizer runs were combined as a fixed effect for each participant.

The functional ROIs were defined within each participant's non-normalized individual space. The uncorrected z-contrast map was thresholded at 1.64 (corresponding to $p < 0.05$). The ROIs were created in two steps. In the first step the ROIs were defined manually from the thresholded z-contrast map. In the second step, the top 50 voxels with the highest z-contrast within each ROI on each side of the brain were selected for the final ROIs. All ROIs were combined into unified bilateral ROIs. Each bilateral ROI therefore consisted of 100 voxels. The PPA, RSC, and OPA were defined from the scenes versus objects contrast, while the LOC was defined from the objects versus scrambled objects contrast.

The hippocampus ROI was defined anatomically from each participant's T1 structural image. Each participant's structural image was preprocessed by FreeSurfer (Martinos Center for Biomedical Imaging, Charlestown, MA; Dale et al., 1999). The hippocampus ROI was extracted from FreeSurfer's automated anatomical segmentation. Each

hippocampus ROI was then manually split by a coronal plane into anterior and posterior ROIs with approximately equal numbers of voxels. On average, the bilateral anterior hippocampus contained 105 voxels, while the bilateral posterior hippocampus included 101 voxels. Then each bilateral ROI was further separated into unilateral ROIs.

2.7. MVPA classification

The ROI-based MVPA analysis was carried out based on the ROIs and the normalized PE maps. First, a classification on object shapes was conducted. The classification accuracy was calculated for each ROI in each participant. A leave-one-run-out cross-validation procedure was used. Within each fold, a linear discriminant analysis (LDA) classifier was trained on five runs to classify between the multivariate patterns of the eight objects (8-way classification) and then applied to the left-out run to generate the classification accuracy score. Six such folds were implemented. The overall accuracy of the classification was calculated by averaging the accuracies from all six folds. Then, the group-level accuracy for each ROI was calculated by averaging classification accuracies across participants. The classification procedures were implemented by the CoSMoMVPA toolbox (Oosterhof et al., 2016).

For statistical inference, a permutation procedure was conducted for each participant. For each permutation, the object labels were shuffled. Then, a random accuracy score based on the permuted labels was calculated by the same classification procedure described above. The permutation procedure was repeated 100 times for each ROI within each participant.

At the group level, a bootstrap procedure was implemented to generate the group-level null distribution of the mean accuracies. For each bootstrap, 1 of the 100 random accuracies was randomly picked from each participant's permutation distribution. Then, the group mean accuracy was calculated by averaging the selected accuracies across participants. This bootstrap procedure was repeated 10,000 times. Then, each ROI ended up with a group-level empirical null distribution (n = 10,000). By comparing the actual group mean accuracy to the null distribution, the p-value for each ROI on the group level could be calculated. Since this test was to determine whether the classification accuracy for different object shapes was significantly above chance, a one-tailed p-value was calculated ($p < 0.05$ was considered significant). This statistical inference procedure is adapted from the method described by Stelzer et al. (2013). All p-values were adjusted for multiple comparisons across 21 unilateral and bilateral ROIs by the false discovery rate (FDR) method (Benjamini and Hochberg, 1995).

The second ROI-based classification aimed to identify the brain regions encoding object locations. The analysis procedure was similar to that used for object shape classification. However, for this analysis, the classifier was trained on four objects, one from each room, and then tested on the other four objects. Classification accuracies from all possible combinations of training and testing object sets were calculated and then averaged. The same statistical inference procedure was applied. This 4-way cross-classification analysis excluded possible confounds from object shapes, since theoretically a shape classifier trained on one set of shapes would have difficulty to classify a novel set of shapes. In this way, the only association between objects in the training set and objects in the testing set was their spatial location, or the room in which they were co-located.

For all the classification analyses described above, changes in classification accuracies from pre to post were also calculated by subtracting accuracies in the pre-session from the post-session. For the statistical inference, at the permutation step, data from both sessions were assigned with the same permutated labels. Then, the accuracy difference was calculated for each permutation. In addition, since the test here was to see whether there was a significant change in classification accuracy from pre to post, a two-tailed p-value was calculated ($p < 0.05$ was considered significant).

2.8. Searchlight analysis

A whole-brain searchlight analysis was conducted to look for possible neural representation of landmark objects outside the pre-defined ROIs. The same location classification was carried out in each searchlight with a radius of 3 voxels based on the post learning data. Then each individual's accuracy change map was converted into normalized MNI152 space. As an exploratory analysis, one-sample t-test was conducted for statistical inference. Threshold-free cluster enhancement (TFCE) at 5 mm was also applied (Smith and Nichols, 2009)

3. Results

Participants needed two to five training sessions to reach an accuracy of 100% on both testing tasks. The first 2 training sessions were mandatory. All training sessions were conducted on different days within two weeks. Two participants needed 4–5 training sessions. Three participants needed 3 training sessions. The majority, thirteen participants, needed 2 training sessions.

With the localizer procedure described above, LOC, PPA, and OPA could be identified in 17 participants. RSC could be defined in 18 participants. The hippocampus was defined structurally in all 18 participants. See Fig. 3 for ROI locations in an example participant. ROI-based analyses were carried out in each participant's native space. The coordinates of all ROIs in MNI space are shown in Table S2.

The classification of object shapes was carried out separately for the pre and post fMRI sessions. The chance level for an 8-way classification is 12.5% (dotted line in Fig. 4). All p-values reported were FDR-corrected across the whole set of 21 ROIs. We first looked at bilateral cortical ROIs (Fig. 4a). Object shapes could be decoded from both pre and post sessions in LOC (pre: mean accuracy = 45.1%, corrected $p < .001$; post: mean accuracy = 52.7%, corrected $p < .001$) and OPA (pre: mean accuracy = 23.9%, corrected $p < .001$; post: mean accuracy = 24.8%, corrected $p < .001$). After training, object shapes could also be decoded from PPA (mean accuracy = 17.8%, corrected $p < .001$). A significant increase of classification accuracy was observed in LOC (mean accuracy change = +7.6%, corrected $p = .004$).

Then the object shape classification was carried out in the unilateral cortical ROIs (Fig. 4b). For the pre session, object shapes could be decoded significantly above chance in left LOC (mean accuracy = 29.5%, corrected $p < .001$), right LOC (mean accuracy = 38.1%, corrected $p < .001$), left OPA (mean accuracy = 21.2%, corrected $p < .001$), and right OPA (mean accuracy = 17.3%, corrected $p < .001$). For the post session, the same pattern of above-chance decoding was observed (left LOC: mean accuracy = 34.1%, corrected $p < .001$; right LOC: mean accuracy = 37.4%, corrected $p < .001$; left OPA: mean accuracy = 23.3%, corrected $p < .001$; right OPA: mean accuracy = 21.1%, corrected $p < .001$). No significant differences in classification accuracy between pre and post sessions were found (all corrected $ps > .05$). No significant decoding or changes in classification accuracies could be identified in any subregion of the hippocampus (all corrected $ps > .05$; Fig. 4c).

The object location classification was conducted using the same procedure as for shape classification. The chance level for this 4-way classification is 25% (dotted lines in Fig. 5). All p-values reported were FDR-corrected across the whole set of 21 ROIs. In the pre session, locations could not be decoded in any of the ROIs (all corrected $ps > .05$). In the post session, there was no significant decoding in any bilateral cortical ROIs (all corrected $ps > .05$; Fig. 5a). However, in unilateral cortical ROIs, locations could be decoded in right PPA (mean accuracy = 28.9%, corrected $p = .048$) and right RSC (mean accuracy = 28.2%, corrected $p = .048$; Fig. 5b). A significant increase of classification accuracy in right PPA was also observed (mean accuracy change = +6.7%, corrected $p = .017$). In the hippocampal ROIs, significant location coding could be found in the bilateral hippocampus (mean accuracy = 28.7%, corrected $p = .048$) and left anterior hippocampus (mean accuracy = 28.2%, corrected $p = .049$; Fig. 5c). No other subre-

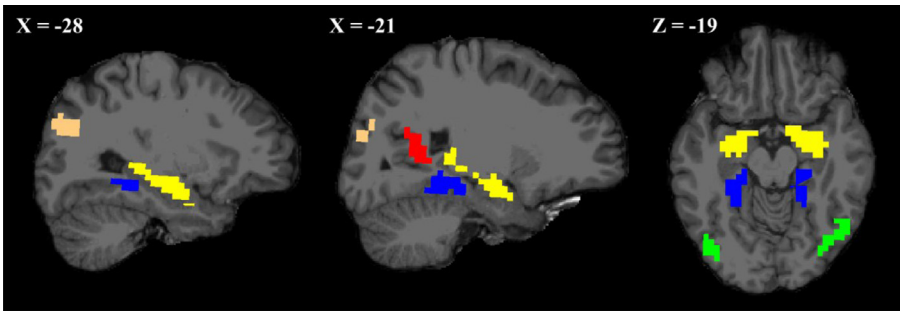

Fig. 3. Region-of-interest location in an example participant. The location of PPA (blue), RSC (red), OPA (orange) and the hippocampus (yellow) is shown in the left and middle slices (overlaid on the high-resolution anatomical scan of the participant's brain). Furthermore, the location of the LOC (green), PPA (blue) and the hippocampus (yellow) are shown in the right slice.

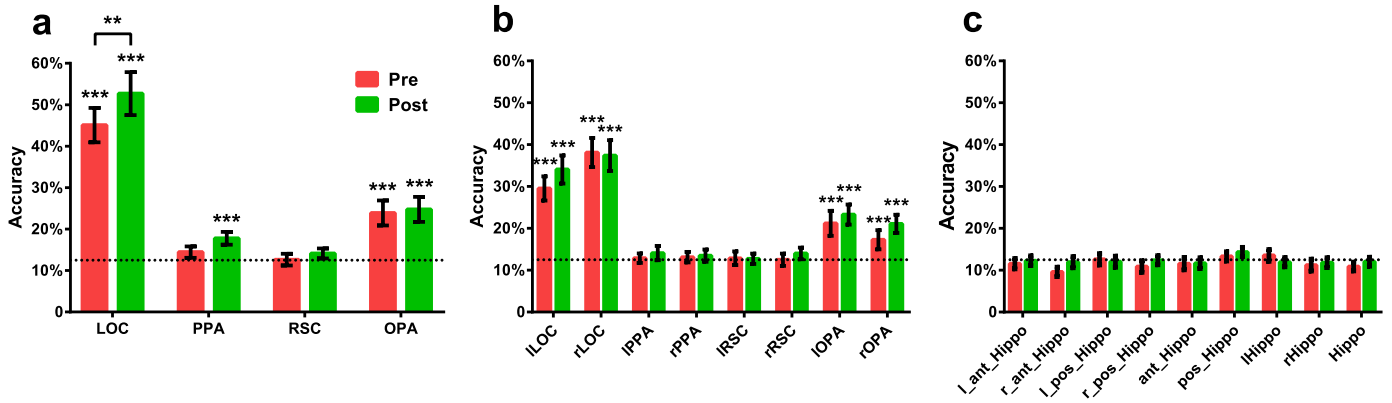

Fig. 4. *Classification accuracies for object shape in bilateral cortical ROIs (a), unilateral cortical ROIs (b), and hippocampal ROIs (c). Red bars show mean accuracies across participants from the pre training session, while green bars show mean accuracies across participants from the post training session (Hippocampus, RSC: n = 18; LOC, PPA, OPA: n = 17). Error bars show standard error of the mean (SEM). Dotted lines represent the chance level (12.5% for 8-way shape classification). Statistical results were corrected for multiple comparisons by means of FDR correction.* ** *p < .01,* *** *p < .001. Labels of unilateral ROIs are prefixed with "l" for left and "r" for right. l_ant_Hippo, left anterior hippocampus; r_ant_Hippo, right anterior hippocampus; l_pos_Hippo, left posterior hippocampus; r_pos_Hippo, right posterior hippocampus; ant_Hippo, anterior Hippocampus; pos_Hippo, posterior Hippocampus; Hippo, bilateral hippocampus.*

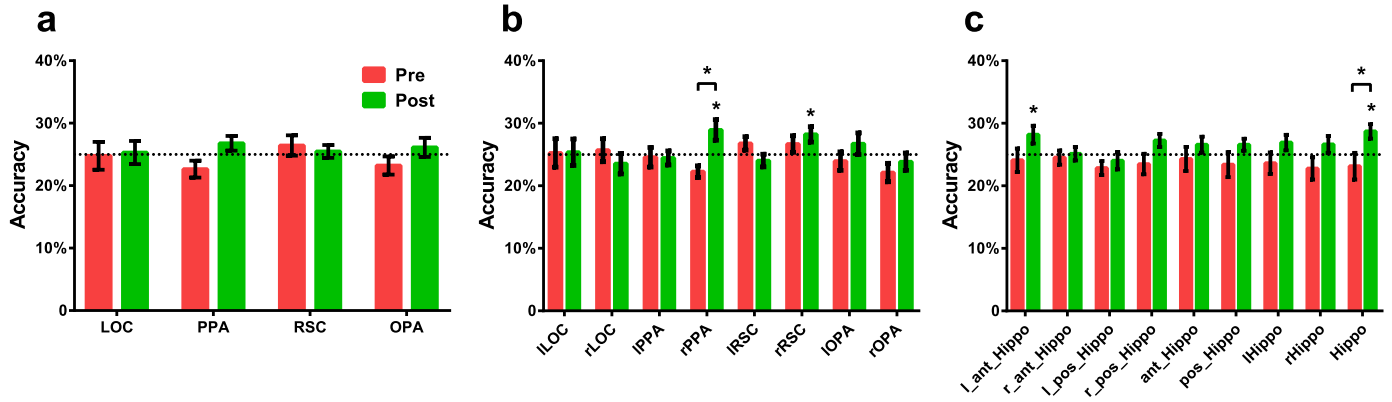

Fig. 5. *Classification accuracies for object location in bilateral cortical ROIs (a), unilateral cortical ROIs (b), and hippocampal ROIs (c). Dotted lines represent the chance level (25% for 4-way location classification). Statistical results were corrected by FDR correction. Otherwise same as Fig. 4.* * *p < .05.*

gions of the hippocampus contained location information (all corrected *p*s > .05). There was a significant increase of classification accuracy in the bilateral hippocampus (mean accuracy change = +5.6%, corrected $p = .036$).

An exploratory searchlight analysis based on the post learning data was conducted to look at possible object location encoding outside the pre-defined ROIs. With an uncorrected threshold of $p < 0.05$, locations of the landmark objects could be decoded from left inferior frontal gyrus, left inferotemporal (IT) cortex (Fig. 6a), left anterior hippocampus, left PPA (Fig. 6b), right PPA (Fig. 6c), and bilateral precuneus cortex (Fig. 6d). Thus, the searchlight analysis supported the coding of landmark locations in the left anterior hippocampus and PPA found in ROI analysis, while suggesting that the left anterior frontal gyrus, left IT and precuneus might also play a role in landmark coding that should be explored in future studies.

4. Discussion

In this study we identify a neural mechanism that the human brain uses to encode the spatial significance of landmark objects in an indoor environment. Participants learned a virtual environment outside the scanner, and brain activity in response to the landmark objects was measured before and after learning. Our results show that learning changed the neural representation of the landmark objects in the hippocampus and right PPA. Specifically, multivoxel BOLD response patterns became more distinguishable for objects in different rooms compared to objects

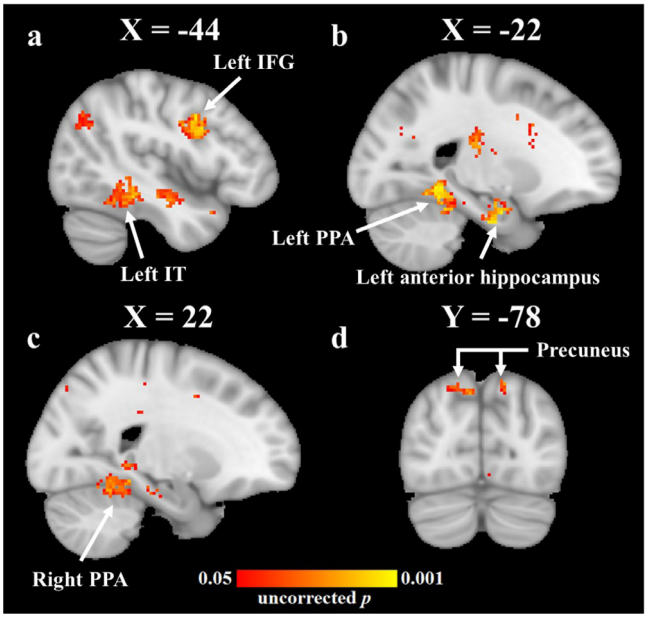

Fig. 6. Results of the searchlight analysis in FSL MNI152 space across participants (n = 18). Object location coding could be found in a) left inferior frontal gyrus (IFG), left inferotemporal (IT) cortex, b) left anterior hippocampus, left PPA, c) right PPA, and d) bilateral precuneus cortex.

in the same room. This suggests that these regions learned to encode the objects based on their navigational significance: they encoded the places associated with the objects.

Our results for the human hippocampus agree with previous findings showing that the hippocampus encodes spatial locations in both rodents (O'Keefe and Nadel, 1978; Moser et al., 2008) and humans (Burgess et al., 2002). For example, previous fMRI studies have found that the hippocampus exhibits distance-dependent adaptation effect between buildings on a college campus (Morgan et al., 2011) and distance-dependent multivoxel pattern similarity for objects encountered within a virtual city (Deuker et al., 2016; see also Nielson et al., 2015). The study by Deuker and colleagues is particularly relevant, because they scanned their participants both before and after environmental learning, and thus they were able to show that the object representations within the hippocampus changed as a result of learning. For indoor spaces, a recent study (Kim and Maguire, 2018) examined fMRI adaptation effects while participants viewed movies showing navigation to paintings located in fixed positions in a multi-room building and performed a spatial memory task on these paintings. They found that the left anterior hippocampus showed fMRI adaptation related to repetition of similar locations across rooms on successive trials, while posterior hippocampus, PPA, and RSC showed adaptation related to repetition of locations in the same room. Our results are consonant with their findings in that the hippocampus and PPA encode spatial locations, but go beyond them by showing location-related activation patterns that are elicited by the landmark objects themselves, even when participants do not perform a spatial memory task.

Notably, all these previous studies used a rich environment in which many different geometric features and objects could be used for orientation. In contrast, we used a sparse environment in which the objects were, by design, the essential navigational cues. Thus, we can be confident that the objects we examined were used as landmarks. Our study is therefore the first to demonstrate conclusively that the spatial representation of learned landmark objects in the hippocampus and right PPA (and possibly also right RSC) automatically arises by exposure to the objects, thus suggesting that associations between the objects and their spatial locations had been formed by training.

We also observed landmark effects in scene regions. Like the hippocampus, right PPA exhibited a change in object representations, such that the room that each object was located in could be decoded from fMRI response patterns after learning. Right RSC also exhibited a room effect after learning, though in this region the change from pre to post learning was not significant. The PPA and RSC have been previously shown to exhibit enhanced responses to objects with qualities that would make them more suitable as landmarks (Troiani et al., 2014), such as being large in size (Konkle and Oliva, 2012), fixed in space (Auger et al., 2015, 2012; Auger and Maguire, 2013), or associated with navigationally relevant locations (Janzen and van Turennout, 2004; Schinazi and Epstein, 2010). Furthermore, parahippocampal cortex has been shown to respond more strongly when participants navigate through environments with landmarks compared to environments that do not contain landmarks (Maguire et al, 1998). These findings indicate that PPA and RSC respond to objects that can potentially be associated with specific locations (or headings), but they did not actually demonstrate the existence of an object-spatial association, as we do here. Previous studies have also shown that multivoxel activation patterns in these regions (along with OPA) generalize across exterior and interior views of the same building, suggesting that they code either landmark identity or landmark location (Marchette et al., 2015). The current results cannot be explained in terms of coding of landmark identity, because the landmarks in the same room were distinct objects with different visual and shape features that were never seen at the same time. Thus, we conclude that right PPA (and possibly also right RSC) represents the location associated with the landmark.

We did not observe any effect on encoding spatial significance of landmark objects in OPA. Previous work has primarily implicated OPA in the encoding of the geometric structure of local spaces (Epstein and Baker, 2019). For example, Kamps et al. (2016) demonstrated that OPA encoded the boundaries of local spaces, and Julian et al. (2016) found that processing of these boundaries was interrupted by inhibitory transcranial magnetic stimulation to OPA. Using multivoxel pattern analysis, Bonner and Epstein (2017) reported that OPA also participated in the coding of navigational affordances, which was defined as the pattern of pathways one could take in a local space, while Henriksson et al. (2019) found that it represented the layout of bounding surfaces. These findings suggest that OPA is more involved in the encoding of the internal spatial structure of scenes rather than the encoding of the spatial significance of landmark objects.

Our findings with landmarks are reminiscent of previous work showing that scene regions encode associations between different views observable from the same location. Robertson et al. (2016) showed that different scene views at the same location learned from a continuous panoramic experience elicited similar multivoxel patterns in RSC and OPA, while Berens et al. (2021) found that representations of scene views from the same location became similar in PPA and RSC after learning. Furthermore, Berens et al. (2021) found that this location representation in RSC was only present when participants could explicitly identify two scenes as views from the same location. In contrast, such a representation in PPA was independent of participants' explicit memory. Their results, together with our findings, indicate that the location coding for scenes and landmark objects might have shared neural mechanisms in PPA and RSC. Our results are also consistent with the associative processing function of scene regions proposed by Aminoff et al. (2007; also see Aminoff and Tarr, 2015), insofar as we find evidence that the PPA encodes an association between landmark objects and their spatial contexts (rooms).

What is the nature of the landmark location codes in the hippocampus and scene regions? There are two possibilities. First, these regions might support a "spatial" map of the environment, in which distances and directions between locations are represented. Second, they may simply represent locations as distinct "places", without encoding any spatial relationships between them. Previous work has found evidence for coding of spatial relationships between locations in the hippocampus

(Deuker et al., 2016; Howard et al., 2014; Morgan et al., 2011) and RSC (Marchette et al., 2014), but not PPA (Persichetti and Dilks, 2019; although see Sulpizio et al., 2014). More broadly, previous work has implicated hippocampus and RSC in the mediation of the spatial aspects of a "cognitive map" whereas PPA is implicated in the recognition of individual places or contexts within the map (Epstein et al., 2017; Julian et al., 2018). To see if we observe a similar division of labor in the current data, we examined the confusion matrix of the 4-way object location classification. Our hypothesis was that if the representation we found was based on a spatial map or any representation with distance information, then there should be more classification errors between objects in neighboring rooms compared to errors between objects in distant (diagonal) rooms, since the former objects were spatially closer than the latter. We used the mean difference between the counts of these two errors as the measure and did the same bootstrapping test as in the accuracy analysis. We did not find any significant effect in either the hippocampus or the PPA (all $ps > .05$; Fig. S2). These null results are most consistent with a categorical spatial code in both regions, but we interpret them with caution, because our environment was suboptimal for examining map-like representations due to the minimal variation in between-room distances.

The landmark location codes found in the current study were independent of the representation of object shape. We could decode object shapes individually in LOC and OPA both before and after training, but we observed no significant decoding in the two regions when the objects were classified according to their locations. LOC is a major cortical hub for object shape processing (Grill-Spector et al., 2001; Konen and Kastner, 2008; Malach et al., 1995), and a previous study found that object category (which relates to shape) could be decoded in both LOC and OPA (Julian et al., 2017). An open question for future research is how these object identity codes in LOC and OPA get bound to object location codes in hippocampus and OPA. In addition, there was a significant increase of object classification accuracy from pre learning to post learning in LOC. We suspect that this is due to increased object familiarity after learning.

In our study, among 18 participants, two participants needed 4–5 training sessions in order to learn the space. In a correlation analysis, we found that the number of training sessions was positively correlated with the increase of the object location classification accuracy in right PPA across participants ($r = 0.55$, $p = 0.021$), though this result did not survive FDR correction. Nevertheless, this result indicates that more extensive training might have reinforced the spatial representations observed in right PPA. Of note, we have very limited variability in our sample (only 2 participants took 4–5 training sessions, whereas most participants finished within two training sessions). Therefore, future studies should use a larger sample size to investigate the possible association between the amount of training and the magnitude of the learning effect.

Furthermore, there is a possibility that the group-level result was primarily driven by the location effect observed in the participants with extensive training. To test this, the same object location classification was conducted based on the participants who needed only 2–3 training sessions, excluding the two participants who required 4–5 training sessions. We were able to replicate our findings (Fig. S1) with less significant results (no ROI survived FDR correction), presumably due to the reduced sample size ($n = 16$) with reduced statistical power. In sum, the effects we observed stood even if we only included participants with 2–3 sessions of training.

There were some limitations in the current study. In our design, all objects were landmarks fixed in space. There was no direct comparison between landmark objects and non-landmark objects. Auger et al. (2015) observed increased activity in scene regions for permanent landmark objects but not for transient non-landmark objects while participants were learning the layout of an environment. In future studies, it would be informative to test whether the representational changes we observed only happened for landmark objects, but not for objects that cannot be landmarks because they are not reliably associated with a specific location.

In addition, some effects we observed showed discrepancy between bilateral ROI results and unilateral ROI results. On one hand, this could be because some effects might only involve one hemisphere but not the other (e.g. rPPA). On the other hand, it could be caused by the high noise level. Decoding accuracy in bilateral ROIs might be facilitated because of the larger number of voxels relative to unilateral ROIs. For example, in the object location classification, significant decoding of locations was found in the bilateral hippocampus and left anterior hippocampus. However, the pattern of decoding accuracies across the four subregions of the hippocampus (Fig. 5c), including left anterior hippocampus, left posterior hippocampus, right anterior hippocampus, and right posterior hippocampus, showed a trend of significant post-learning decoding (27.3%) as well as an accuracy increase (+3.8%) in right posterior hippocampus. This indicated the possibility that location information might be coded in both left anterior hippocampus and right posterior hippocampus, which contributed to the significant decoding of locations in the bilateral hippocampus. However, future studies are needed to test this possibility directly.

In summary, our results reveal a neural representation of landmark objects in the hippocampus and right PPA based on their locations in indoor spaces. Future studies are needed to investigate the nature of such location representations in different brain regions and how they coordinate with each other during navigation.

Data and code availability

The data used in this manuscript is available upon request with the need for a formal data sharing agreement.

The custom scripts used in this study are available at https://github.com/bearsun/landmark_paper.

Declaration of Competing Interest

The authors declare that they have no competing interests.

Credit authorship contribution statement

Liwei Sun: Conceptualization, Methodology, Software, Investigation, Data curation, Formal analysis, Writing - original draft, Visualization. **Sebastian M. Frank:** Conceptualization, Investigation, Writing - review & editing. **Russell A. Epstein:** Resources, Writing - review & editing. **Peter U. Tse:** Conceptualization, Writing - review & editing, Supervision, Funding acquisition.

Acknowledgements

This research was supported by a grant from the NSF (1632738 to P.U.T.).

Supplementary materials

Supplementary material associated with this article can be found, in the online version, at doi:10.1016/j.neuroimage.2021.118081.

References

Aguirre, G.K., Mattar, M.G., Magis-Weinberg, L., 2011. De Bruijn cycles for neural decoding. Neuroimage 56, 1293–1300. doi:10.1016/j.neuroimage.2011.02.005.

Aminoff, E., Gronau, N., Bar, M., 2007. The parahippocampal cortex mediates spatial and nonspatial associations. Cereb. Cortex 17, 1493–1503. doi:10.1093/cercor/bhl078.

Aminoff, E.M., Tarr, M.J., 2015. Associative processing is inherent in scene perception. PLoS One 10, 1–19. doi:10.1371/journal.pone.0128840.

Auger, S.D., Maguire, E.A., 2013. Assessing the mechanism of response in the retrosplenial cortex of good and poor navigators. Cortex 49, 2904–2913. doi:10.1016/j.cortex.2013.08.002.

Auger, S.D., Mullally, S.L., Maguire, E.A., 2012. Retrosplenial cortex codes for permanent landmarks. PLoS One 7. doi:10.1371/journal.pone.0043620.

Auger, S.D., Zeidman, P., Maguire, E.A., 2015. A Central Role for the Retrosplenial Cortex in de Novo Environmental Learning eLife 4. doi:10.7554/eLife.09031.
Benjamini, Y., Hochberg, Y., 1995. Controlling the false discovery rate: a practical and powerful approach to multiple testing. J. R. Stat. Soc. 57, 289–300. doi:10.1111/j.2517-6161.1995.tb02031.x.
Berens, S.C., Joensen, B.H., Horner, A.J., 2021. Tracking the emergence of location-based spatial representations in human scene-selective cortex. J. Cognit. Neurosci. 33, 445–462. doi:10.1162/jocn_a_01654.
Bonner, M.F., Epstein, R.A., 2017. Coding of navigational affordances in the human visual system. Proc. Natl. Acad. Sci. 114, 4793–4798. doi:10.1073/pnas.1618228114.
Burgess, N., Maguire, E.A., O'Keefe, J., 2002. The human hippocampus and spatial and episodic memory. Neuron 35, 625–641. doi:10.1016/S0896-6273(02)00830-9.
Chan, E., Baumann, O., Bellgrove, M.A., Mattingley, J.B., 2012. From objects to landmarks: the function of visual location information in spatial navigation. Front. Psychol. 3. doi:10.3389/fpsyg.2012.00304.
Connolly, A.C., Sha, L., Swaroop Guntupalli, J., Oosterhof, N., Halchenko, Y.O., Nastase, S.A., Castello, M.V., di, O., Abdi, H., Jobst, B.C., Ida Gobbini, M., Haxby, J.v., 2016. How the human brain represents perceived dangerousness or "predacity" of animals. J. Neurosci. 36, 5373–5384. doi:10.1523/JNEUROSCI.3395-15.2016.
Dale, A.M., Fischl, B., Sereno, M.I., 1999. Cortical surface-based analysis: I. Segmentation and surface reconstruction. Neuroimage 9, 179–194. doi:10.1006/nimg.1998.0395.
Deuker, L., Bellmund, J.L., Navarro Schröder, T., Doeller, C.F., 2016. An Event Map of Memory Space in the Hippocampus. eLife 5, e16534 doi:10.7554/eLife.16534.
Epstein, R., Kanwisher, N., 1998. A cortical representation of the local visual environment. Nature 392, 598–601. doi:10.1038/33402.
Epstein, R.A., Baker, C.I., 2019. Scene perception in the human brain. Annu. Rev. Vis. Sci. 5, 373–397. doi:10.1146/annurev-vision-091718-014809.
Epstein, R.A., Patai, E.Z., Julian, J.B., Spiers, H.J., 2017. The cognitive map in humans: spatial navigation and beyond. Nat. Neurosci. 20, 1504–1513. doi:10.1038/nn.4656.
Faul, F., Erdfelder, E., Lang, A.G., Buchner, A., 2007. G*Power 3: a flexible statistical power analysis program for the social, behavioral, and biomedical sciences. Behav. Res. Methods 39, 175–191. doi:10.3758/BF03193146.
Grill-Spector, K., Kourtzi, Z., Kanwisher, N., 2001. The lateral occipital complex and its role in object recognition. Vis. Res. 41, 1409–1422. doi:10.1016/S0042-6989(01)00073-6.
Haxby, J.V., Gobbini, M.I., Furey, M.L., Ishai, A., Schouten, J.L., Pietrini, P., 2001. Distributed and overlapping representations of faces and objects in ventral temporal cortex. Science 293, 2425–2430. doi:10.1126/science.1063736.
Henriksson, L., Mur, M., Kriegeskorte, N., 2019. Rapid invariant encoding of scene layout in human OPA. Neuron 103, 161–171. doi:10.1016/j.neuron.2019.04.014, e3.
Howard, L.R., Javadi, A.H., Yu, Y., Mill, R.D., Morrison, L.C., Knight, R., Loftus, M.M., Staskute, L., Spiers, H.J., 2014. The hippocampus and entorhinal cortex encode the path and euclidean distances to goals during navigation. Curr. Biol. 24, 1331–1340. doi:10.1016/j.cub.2014.05.001.
Janzen, G., van Turennout, M., 2004. Selective neural representation of objects relevant for navigation. Nat. Neurosci. 7, 673–677. doi:10.1038/nn1257.
Jenkinson, M., Bannister, P., Brady, M., Smith, S., 2002. Improved optimization for the robust and accurate linear registration and motion correction of brain images. Neuroimage 17, 825–841. doi:10.1006/nimg.2002.1132.
Jenkinson, M., Beckmann, C.F., Behrens, T.E.J., Woolrich, M.W., Smith, S.M., 2012. FSL. NeuroImage 62, 782–790. doi:10.1016/j.neuroimage.2011.09.015.
Jenkinson, M., Smith, S., 2001. A global optimisation method for robust affine registration of brain images. Med. Image Anal. 5, 143–156. doi:10.1016/S1361-8415(01)00036-6.
Julian, J.B., Keinath, A.T., Marchette, S.A., Epstein, R.A., 2018. The neurocognitive basis of spatial reorientation. Curr. Biol. 28, R1059–R1073. doi:10.1016/j.cub.2018.04.057.
Julian, J.B., Ryan, J., Epstein, R.A., 2017. Coding of object size and object category in human visual cortex. Cereb. Cortex 27, 3095–3109. doi:10.1093/cercor/bhw150.
Julian, J.B., Ryan, J., Hamilton, R.H., Epstein, R.A., 2016. The occipital place area is causally involved in representing environmental boundaries during navigation. Curr. Biol. 26, 1104–1109. doi:10.1016/j.cub.2016.02.066.
Kamps, F.S., Julian, J.B., Kubilius, J., Kanwisher, N., Dilks, D.D., 2016. The occipital place area represents the local elements of scenes. Neuroimage 132, 417–424. doi:10.1016/j.neuroimage.2016.02.062.
Kim, M., Maguire, E.A., 2018. Hippocampus, retrosplenial and parahippocampal cortices encode multicompartment 3d space in a hierarchical manner. Cereb. Cortex 28, 1898–1909. doi:10.1093/cercor/bhy054.
Konen, C.S., Kastner, S., 2008. Two hierarchically organized neural systems for object information in human visual cortex. Nat. Neurosci. 11, 224–231. doi:10.1038/nn2036.
Konkle, T., Oliva, A., 2012. A real-world size organization of object responses in occipitotemporal cortex. Neuron 74, 1114–1124. doi:10.1016/j.neuron.2012.04.036.
Maguire, E.A., Frith, C.D., Burgess, N., Donnett, J.G., O'Keefe, J., 1998. Knowing where things are: Parahippocampal involvement in encoding object locations in virtual large-scale space. J. Cognit. Neurosci. 10, 61–76. doi:10.1162/089892998563789.
Malach, R., Reppas, J.B., Benson, R.R., Kwong, K.K., Jiang, H., Kennedy, W.A., Ledden, P.J., Brady, T.J., Rosen, B.R., Tootell, R.B.H., 1995. Object-related activity revealed by functional magnetic resonance imaging in human occipital cortex. Proc. Natl. Acad. Sci. 92, 8135–8139. doi:10.1073/pnas.92.18.8135.
Marchette, S.A., Vass, L.K., Ryan, J., Epstein, R.A., 2015. Outside looking in: Landmark generalization in the human navigational system. J. Neurosci. 35, 14896–14908. doi:10.1523/JNEUROSCI.2270-15.2015.
Marchette, S.A., Vass, L.K., Ryan, J., Epstein, R.A., 2014. Anchoring the neural compass: Coding of local spatial reference frames in human medial parietal lobe. Nat. Neurosci. 17, 1598–1606. doi:10.1038/nn.3834.
Morgan, L.K., MacEvoy, S.P., Aguirre, G.K., Epstein, R.A., 2011. Distances between real-world locations are represented in the human hippocampus. J. Neurosci. 31, 1238–1245. doi:10.1523/JNEUROSCI.4667-10.2011.
Moser, E.I., Kropff, E., Moser, M.B., 2008. Place cells, grid cells, and the brain's spatial representation system. Annu. Rev. Neurosci. 31, 69–89. doi:10.1146/annurev.neuro.31.061307.090723.
Nakamura, K., Kawashima, R., Sato, N., Nakamura, A., Sugiura, M., Kato, T., Hatano, K., Ito, K., Fukuda, H., Schormann, T., Zilles, K., 2000. Functional delineation of the human occipitotemporal areas related to face and scene processing a PET study. Brain 123, 1903–1912. doi:10.1093/brain/123.9.1903.
Nielson, D.M., Smith, T.A., Sreekumar, V., Dennis, S., Sederberg, P.B., 2015. Human hippocampus represents space and time during retrieval of real-world memories. Proc. Natl. Acad. Sci. 112, 11078–11083. doi:10.1073/pnas.1507104112.
O'Craven, K.M., Kanwisher, N., 2000. Mental imagery of faces and places activates corresponding stimulus-specific brain regions. J. Cognit. Neurosci. 12, 1013–1023. doi:10.1162/08989290051137549.
Oosterhof, N.N., Connolly, A.C., Haxby, J.v., 2016. CoSMoMVPA: multi-modal multivariate pattern analysis of neuroimaging data in matlab/GNU octave. Front. Neuroinform. 10. doi:10.3389/fninf.2016.00027.
Persichetti, A.S., Dilks, D.D., 2019. Distinct representations of spatial and categorical relationships across human scene-selective cortex. Proc. Natl. Acad. Sci. 116, 21312–21317. doi:10.1073/pnas.1903057116.
Robertson, C.E., Hermann, K.L., Mynick, A., Kravitz, D.J., Kanwisher, N., 2016. Neural representations integrate the current field of view with the remembered 360° panorama in scene-selective cortex. Curr. Biol. 26, 2463–2468. doi:10.1016/j.cub.2016.07.002.
Schinazi, V.R., Epstein, R.A., 2010. Neural correlates of real-world route learning. Neuroimage 53, 725–735. doi:10.1016/j.neuroimage.2010.06.065.
Smith, S.M., Nichols, T.E., 2009. Threshold-free cluster enhancement: addressing problems of smoothing, threshold dependence and localisation in cluster inference. Neuroimage 44, 83–98. doi:10.1016/j.neuroimage.2008.03.061.
Stelzer, J., Chen, Y., Turner, R., 2013. Statistical inference and multiple testing correction in classification-based multi-voxel pattern analysis (MVPA): random permutations and cluster size control. Neuroimage 65, 69–82. doi:10.1016/j.neuroimage.2012.09.063.
Sulpizio, V., Committeri, G., Galati, G., 2014. Distributed cognitive maps reflecting real distances between places and views in the human brain. Front. Hum. Neurosci. 8. doi:10.3389/fnhum.2014.00716.
Troiani, V., Stigliani, A., Smith, M.E., Epstein, R.A., 2014. Multiple object properties drive scene-selective regions. Cereb. Cortex 24, 883–897. doi:10.1093/cercor/bhs364.
Woolrich, M.W., Ripley, B.D., Brady, M., Smith, S.M., 2001. Temporal autocorrelation in univariate linear modeling of FMRI data. Neuroimage 14, 1370–1386. doi:10.1006/nimg.2001.0931.